nature climate change

ARTICLES

https://doi.org/10.1038/s41558-021-01224-1

Observed increases in extreme fire weather driven by atmospheric humidity and temperature

Piyush Jain[1]✉, Dante Castellanos-Acuna[2], Sean C. P. Coogan[2], John T. Abatzoglou[3] and Mike D. Flannigan[2]

Recent increases in regional wildfire activity have been linked to climate change. Here, we analyse trends in observed global extreme fire weather and their meteorological drivers from 1979 to 2020 using the ERA5 reanalysis. Trends in annual extreme (95th percentile) values of the fire weather index (FWI_{95}), initial spread index (ISI_{95}) and vapour pressure deficit (VPD_{95}) varied regionally, with global increases in mean values of 14, 12 and 12%, respectively. Significant increases occurred over a quarter to almost half of the global burnable land mass. Decreasing relative humidity was a driver of over three-quarters of significant increases in FWI_{95} and ISI_{95}, while increasing temperature was a driver for 40% of significant trends. Trends in VPD_{95} were predominantly associated with increasing temperature. These trends are likely to continue, as climate change projections suggest global decreases in relative humidity and increases in temperature that may increase future fire risk where fuels remain abundant.

Climate and weather greatly influence global wildland fire[1]. Climate influences the type and distribution of vegetation (fuels), and weather is a main driver of regional fire activity[2,3]. Especially important to wildland fire management are the periods of extreme fire weather leading to rapidly spreading fires that are difficult to suppress, often with catastrophic impacts[4]. In fact, a small percentage of fires that occur during extreme fire weather conditions are responsible for the majority of area burned regionally[5,6]. Recent decades have experienced an increase in the number of large and destructive wildfires in many regions[5,7], and nearly all recent extreme wildfire events have occurred under extreme fire weather conditions[8]. In the future, the occurrence of extreme fire weather is expected to increase in many areas due to climate change[9,10].

Extreme fire weather is typically evaluated using fire weather indices that incorporate daily weather variables related to fuel moisture and fire behaviour. Several indices are used across the globe, including the Canadian Fire Weather Index System (CFWIS)[11]. The CFWIS is the most widely used approach for estimation of fire weather globally, both operationally and in a research context. The CFWIS uses meteorological inputs that have been shown to strongly influence the occurrence, behaviour and effects of wildfires including air temperature, relative humidity (RH), wind speed (WS) and precipitation[12,13]. Observed increases in fire weather season length have been found in areas with observed increases in temperature, WS and rain-free intervals, and decreases in RH[14]. Studies using climate models have attributed temperature and RH to projected increased fire weather extremes[10,15]. While regional studies have investigated meteorological drivers of observed trends in fire weather[16–20], the current literature still lacks a global-scale attribution of observed fire weather trends to individual meteorological variables. Such an analysis would greatly improve our knowledge of current and future global fire risk and allow for the identification of high-risk regions with greater potential for catastrophic fires.

This study seeks to investigate trends in extreme fire weather globally from 1979 to 2020, and to elucidate the meteorological variables behind any observed changes. We use the ERA5 reanalysis[21] to estimate and examine trends in extreme values of three different measures of fire weather (Methods): (1) the fire weather index (FWI), (2) initial spread index (ISI) and (3) vapour pressure deficit (VPD). The FWI and ISI are both indices in the CFWIS, where the former provides an estimate of potential fire intensity while the latter represents the potential rate of fire spread. The VPD is the difference between the saturation and actual vapour pressure; high VPD values brought about by the combination of high temperatures and a dry airmass can, over an extended period, result in increased desiccation of fuels. While regional fire regime changes have been further linked to climate change[22,23], the variables driving observed global changes have not been attributed to changes in individual meteorological variables. For this reason, and given the nonlinear nature of the CFWIS, we attribute the dominant meteorological variables responsible for trends in extreme values of ISI and FWI globally. Because RH and VPD are both measures of atmospheric moisture, and both are largely determined by temperature (T) and dew point temperature (Td), we also attribute extreme FWI and ISI trends to VPD and further explore how trends in T and Td combine to influence trends in fire weather extremes.

Global trends in the 95th percentile of FWI, ISI and VPD

We evaluated trends in extreme fire weather by focusing on the 95th percentile of the annual values of FWI, ISI and VPD (denoted henceforth as FWI_{95}, ISI_{95} and VPD_{95}, respectively) from 1979 to 2020 (Methods). We also report these trends according to the global biome classification shown in Supplementary Fig. 1, and use only the fire season estimated for each biome–continent combination to determine annual distributions from which the percentile values were derived. Significant positive trends in annual FWI_{95} occurred in >26.6% of burnable global land mass although there were important regional variations in the observed trends (Fig. 1a, Table 1 and Supplementary Tables 3 and 4). Positive trends in FWI_{95} occurred predominantly in western North America (for example, subtropical

[1]Natural Resources Canada, Canadian Forest Service, Northern Forestry Centre, Edmonton, Alberta, Canada. [2]Department of Renewable Resources, University of Alberta, Edmonton, Alberta, Canada. [3]Management of Complex Systems, University of California, Merced, CA, USA.
✉e-mail: piyush.jain@nrcan-rncan.gc.ca

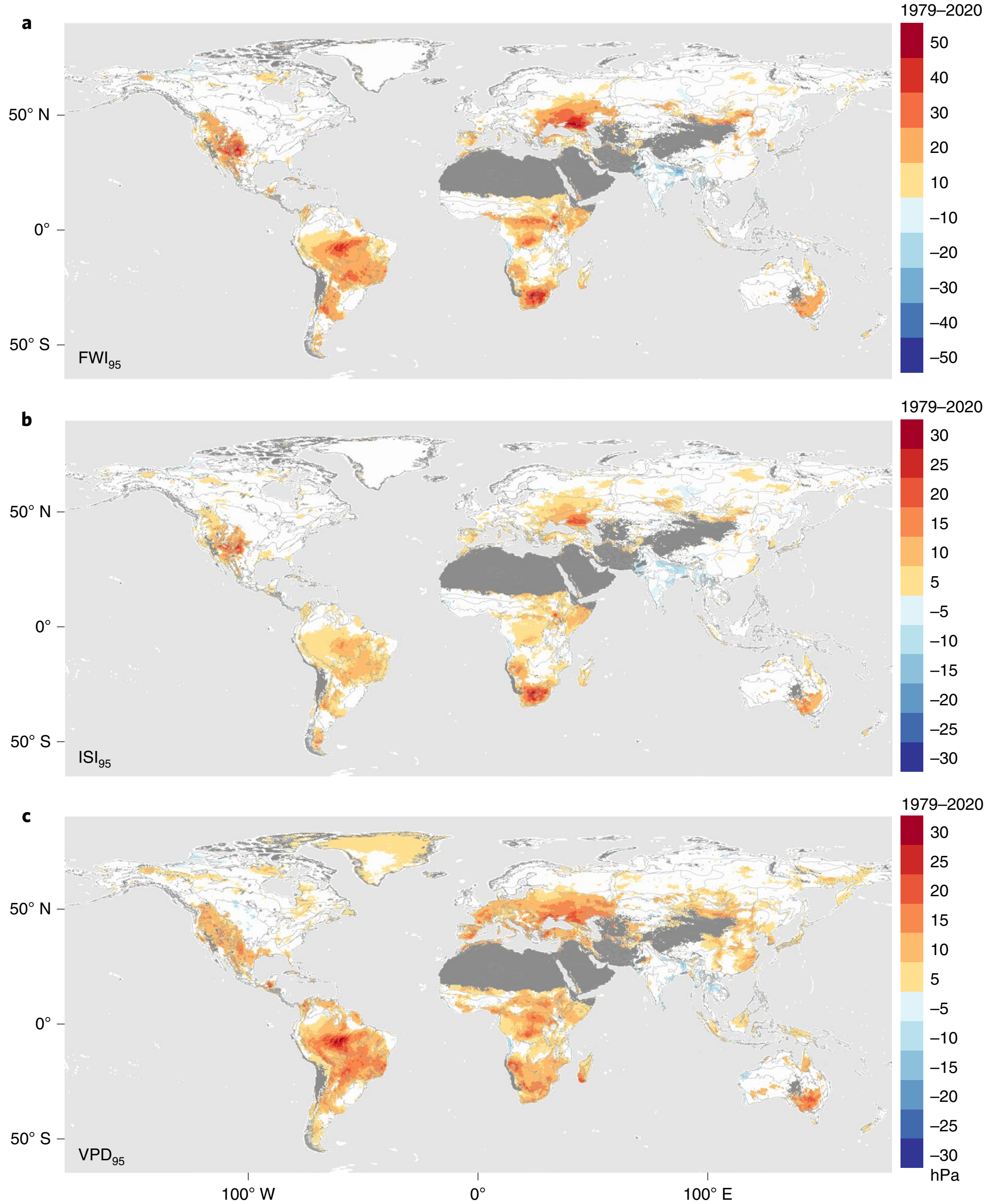

Fig. 1 | Significant trends in extreme fire weather. a–c, Significant trends (1979–2020) in annual FWI_{95} (**a**), ISI_{95} (**b**) and VPD_{95} (**c**). Significance was determined by the MK trend test, controlling for multiple testing and adjusting for spatial autocorrelation ($\alpha = 0.05$). White indicates where no significant trends exist, while dark grey denotes areas predominantly barren (that is, without appreciable burnable biomass), and these are excluded from the calculation. Light grey indicates the boundaries of biomes, which are modified from ref. [50] (Methods). Displayed trends are derived from the Theil–Sen slope estimator. Supplementary Fig. 1 shows an equivalent calculation covering all trends (that is, significant and non-significant).

desert, subtropical mountain system, temperate desert, temperate mountain system west), South America (for example, tropical moist forest south, tropical rainforest), Africa (for example, subtropical mountain system, tropical desert, tropical moist forest north, tropical rainforest), western Europe (for example, subtropical dry forest, temperate continental forest, temperate steppe) and eastern Australia (for example, subtropical dry forest). In contrast, the greatest percentage of negative trends occurred in India (covered predominantly by tropical shrubland and tropical dry forest west biomes). Similar patterns were also seen for trends in annual ISI_{95}, with significant positive trends occurring in >26.4% of global burnable land mass (Fig. 1b and Table 1). In contrast to FWI_{95} and ISI_{95}, significant positive trends in annual VPD_{95} occurred in >45.7% of global burnable lands (Fig. 1c and Table 1), albeit with similar spatial variation. Conversely, significant negative trends in FWI_{95}, ISI_{95} and VPD_{95} were found for <2.5% of global burnable lands, predominantly occurring in India or mainland southeast Asia.

Figure 2 shows the time series of global extreme fire weather anomalies, which are highly correlated with anomalies in global mean land-surface temperatures (Spearman's $\rho > 0.83$). Altogether, for the entire global burnable area the mean value over the 41-year period for FWI_{95} increased by 14.1% (that is, from 29.0 to 33.1) while ISI_{95} increased by 12.0% (from 12.2 to 13.7) and VPD_{95} increased by 12.1% (from 26.4 to 29.6 hPa). Considering only areas that experienced significant trends, the mean changes were larger, corresponding to an increase in mean global FWI_{95}, ISI_{95} and VPD_{95},

Table 1 | Percentages of trends that are significant for all trends (that is, positive and negative), positive trends only and negative trends only, for the three extreme fire weather variables (FWI_{95}, ISI_{95} and VPD_{95}), summarized globally and by continent

	FWI_{95}			ISI_{95}			VPD_{95}		
Percentage significant	**All**	**Positive**	**Negative**	**All**	**Positive**	**Negative**	**All**	**Positive**	**Negative**
Global	28.4	26.6	1.8	28.9	26.4	2.5	47.2	45.7	1.5
By continent									
Africa	54.2	53.1	1.2	50.5	49.1	1.4	76.8	75.7	1.1
Asia	20.6	13.9	6.6	21.9	12.4	9.4	45.9	42.1	3.9
Europe	18.5	17.8	0.7	22.4	20.9	1.5	34.1	33.7	0.4
North America	15.5	14.3	1.2	15.3	14.3	1.0	38.2	36.4	1.8
Oceania	22.9	22.3	0.6	19.5	18.8	0.7	28.7	26.2	2.5
South America	62.6	62.5	0.1	61.7	61.6	0.1	76.9	76.6	0.3
Mean trend size (1979–2020)	**All**	**Positive**	**Negative**	**All**	**Positive**	**Negative**	**All (hPa)**	**Positive (hPa)**	**Negative (hPa)**
Global	4.1 (11.0)	6.3 (12.3)	-2.3 (-8.4)	1.5 (3.9)	2.5 (4.6)	-1.0 (-3.6)	3.2 (5.7)	4.1 (6.0)	-1.8 (-5.3)
By continent									
Africa	7.1 (11.3)	8.1 (11.6)	-1.8 (-5.6)	3.0 (5.1)	3.6 (5.3)	-1.0 (-2.0)	5.2 (6.4)	5.6 (6.5)	-1.9 (-5.1)
Asia	1.1 (3.7)	4.9 (10.2)	-4.1 (-10.0)	0.1 (0.3)	1.9 (3.8)	-1.9 (-4.4)	2.3 (4.4)	3.8 (5.4)	-2.5 (-6.5)
Europe	3.7 (12.3)	5.1 (13.0)	-1.7 (-4.8)	1.1 (3.6)	1.8 (4.0)	-0.7 (-2.0)	3.2 (6.2)	3.6 (6.3)	-1.1 (-1.8)
North America	2.6 (11.6)	5.0 (13.1)	-1.8 (-6.7)	1.1 (4.7)	2.0 (5.3)	-0.7 (-2.7)	1.7 (3.0)	2.3 (3.4)	-1.8 (-4.4)
Oceania	4.7 (11.7)	6.3 (12.2)	-1.8 (-5.6)	2.0 (6.1)	3.3 (6.4)	-1.4 (-3.0)	2.3 (6.5)	4.5 (7.8)	-2.2 (-7.0)
South America	9.0 (12.9)	9.7 (12.9)	-1.3 (-4.4)	3.0 (4.2)	3.3 (4.3)	-0.6 (-1.5)	6.7 (8.3)	7.1 (8.4)	-1.1 (-2.3)

Mean trend sizes (1979–2020) for all grid cells are also given, where values in parentheses are the corresponding mean trend sizes for significant trends only.

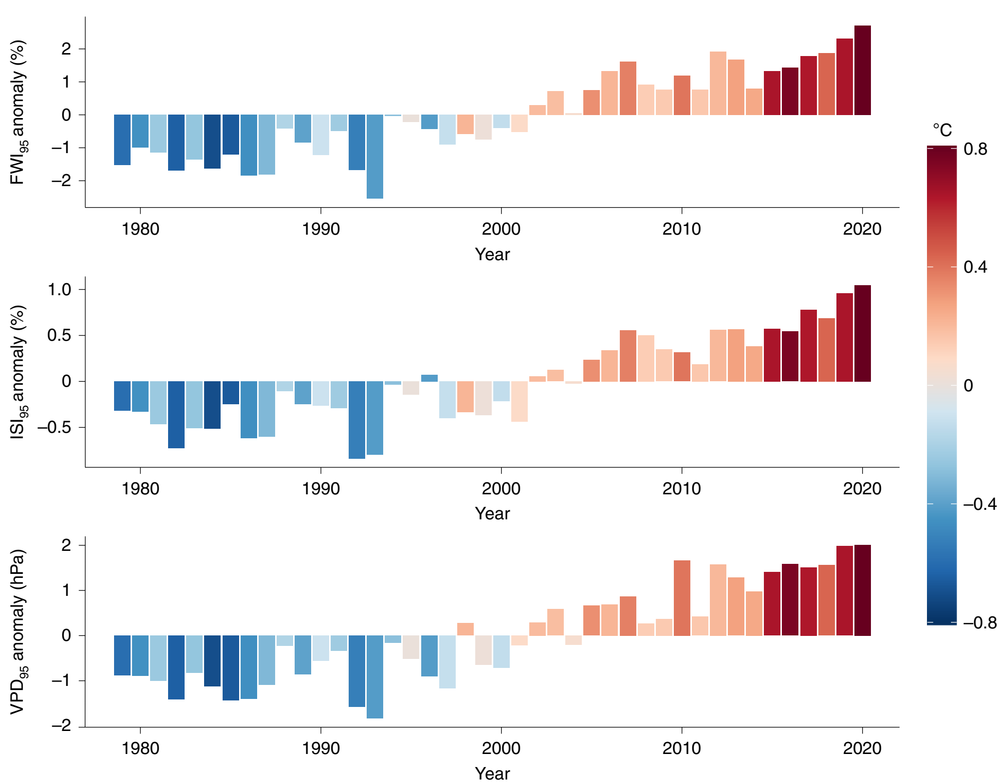

Fig. 2 | Anomalies in annual extreme fire weather metrics. Anomalies in annual (fire season) global means of extreme fire weather metrics (FWI_{95}, ISI_{95} and VPD_{95}) between 1979 and 2020. Each bar is coloured according to annual global mean land-surface temperature anomalies (using data from ref. [29]). All anomalies are calculated relative to the entire period 1979–2020.

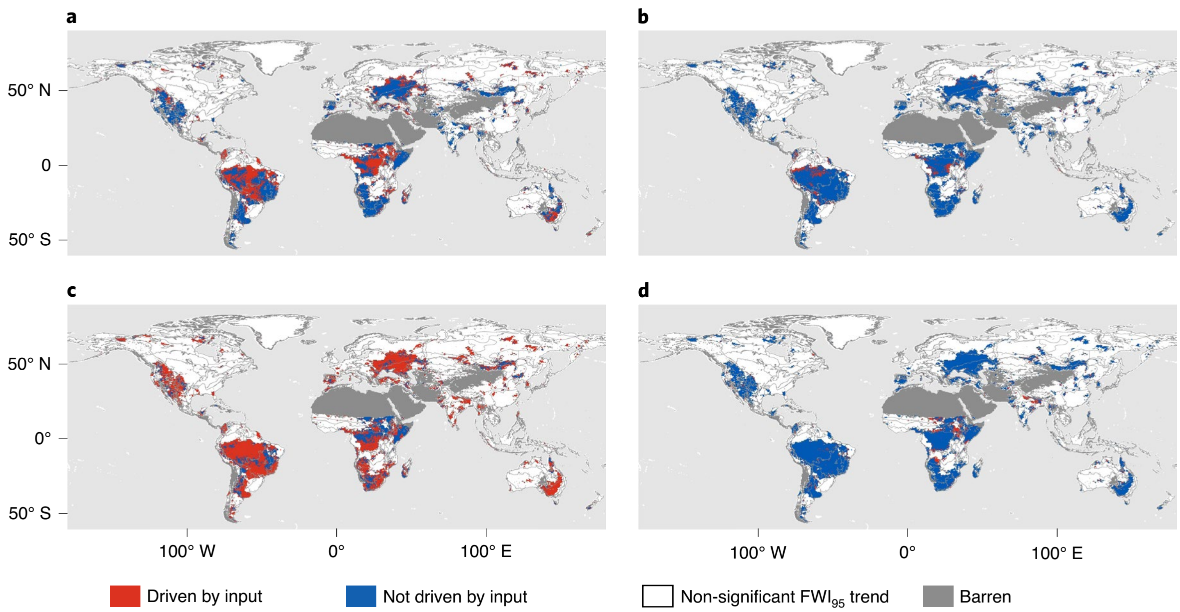

Fig. 3 | Global attribution of FWI_{95} trends. a–d, FWI inputs attributed as drivers of FWI_{95} as determined by an attribution test based on the pMK (Methods). Red indicates where the corresponding FWI system input variable—noon temperature (**a**), daily precipitation (**b**), noon RH (**c**) and noon WS (**d**)—is a driver of the observed significant trend in FWI_{95}. Blue indicates that the corresponding variable is not a driver of the observed significant trends in FWI_{95}, white indicates where trends in FWI_{95} are not significant, dark grey indicates barren (non-burnable) lands excluded from the calculation and light grey indicates the boundaries of biomes, which are modified from ref. [50] (Methods).

of 31.6% (that is, from 34.8 to 45.9), 30.2% (from 13.0 to 16.9) and 20.8% (from 27.3 to 33.0 hPa), respectively (Table 1).

The greatest percentage of significant trends showing increases in FWI_{95}, ISI_{95} and VPD_{95} tended to occur in tropical, subtropical and temperate biomes (Supplementary Tables 2 and 4). It is important to note, however, that extreme wildfire events are generally limited by fuel availability in low-productivity climates and by mesic conditions in very productive climates[8,24], with the latter exhibiting more robust links to variability in FWI and VPD[1]. However, productive tropical ecosystems are an exception because people set fires in these regions for agricultural purposes and to clear rainforest[25]. There were also positive trends in extreme fire weather in boreal ecosystems, although both the significance and size of trends in FWI_{95}, ISI_{95} and VPD_{95} were generally smaller compared with tropical, subtropical and temperate biomes (Supplementary Tables 2, 4 and 5). While the polar biome showed relatively few significant trends in ISI_{95} and FWI_{95}, there were positive trends in VPD_{95} across 39.5% of polar burnable area (Supplementary Table 2). In general, although trends in all three extreme fire weather metrics largely agreed in regard to direction, magnitude and regional variation, there were almost double the number of significant trends in VPD_{95} compared with FWI_{95} and ISI_{95}. This difference is not surprising given the more direct influence of temperature on VPD_{95} than on the other metrics. The more robust increase in VPD extremes may have implications in some regions given its influence on fine fuel flammability[26].

The observed spatial patterns of positive significant trends in historical fire weather extremes shown here are consistent with earlier studies that include the European Mediterranean[27], North America[18] and Australia[28]. Globally, Jolly et al.[14] found significant lengthening of the potential fire season over a quarter of the earth's vegetated surface based on analysis of several fire weather indices between 1979 and 2013. Our analysis, however, is based on the more recent ERA5 reanalysis with higher spatial resolution and an extended period of analysis, from 1979 to 2020, the most recent decade (2011–2020), which contains the seven warmest years over land on global record[29], as well as the recent record-breaking fire seasons in western USA, Siberia, Australia and the Amazon region. We found that the most recent decade also includes the eight most extreme fire weather years globally for FWI_{95} and ISI_{95} and the nine most extreme years for VPD_{95} (Fig. 2). This recent period is therefore likely to have been instrumental in driving extreme fire weather trends congruent with observed global warming.

Trends driven by atmospheric humidity and temperature

To investigate drivers of the observed significant trends in FWI_{95} and ISI_{95}, we conducted a partial Mann–Kendall test (pMK; Methods) where we considered the four CFWIS input variables as covariates (that is, T, precipitation, RH and WS), as well as VPD. The pMK test is a method used for detection of multivariate trends that can ascertain whether a covariate has an influence on the trend of a response variable. If any trend in the response variable that is originally determined to be statistically significant is no longer significant after accounting for the covariate and repeating the test, then the covariate has a significant influence on the detected trend. We refer to such covariates as drivers of a significant trend in the response variable. Using this method, RH and T were identified as the drivers of significant trends in FWI_{95} in more grid cells (Fig. 3) and for more biomes and continents (Fig. 4 and Supplementary Tables 3 and 6) than WS or precipitation. Globally, RH was attributed as a driver of FWI_{95} for 75.0% of grid cells with significant trends, while T, precipitation and WS accounted for 40.4, 11.3 and 10.6% of significant grid cells, respectively. Results for ISI_{95} were quantitatively similar (Supplementary Fig. 6 and Supplementary Tables 3 and 6). By contrast, WS and precipitation were identified as drivers of observed trends in a few, specific parts of the world. The minor role of precipitation identified here may be attributable to the fact that the precipitation increases are not sufficiently large to offset the effects of warming[13] and the stronger links between fire activity and precipitation frequency rather than precipitation amount[12].

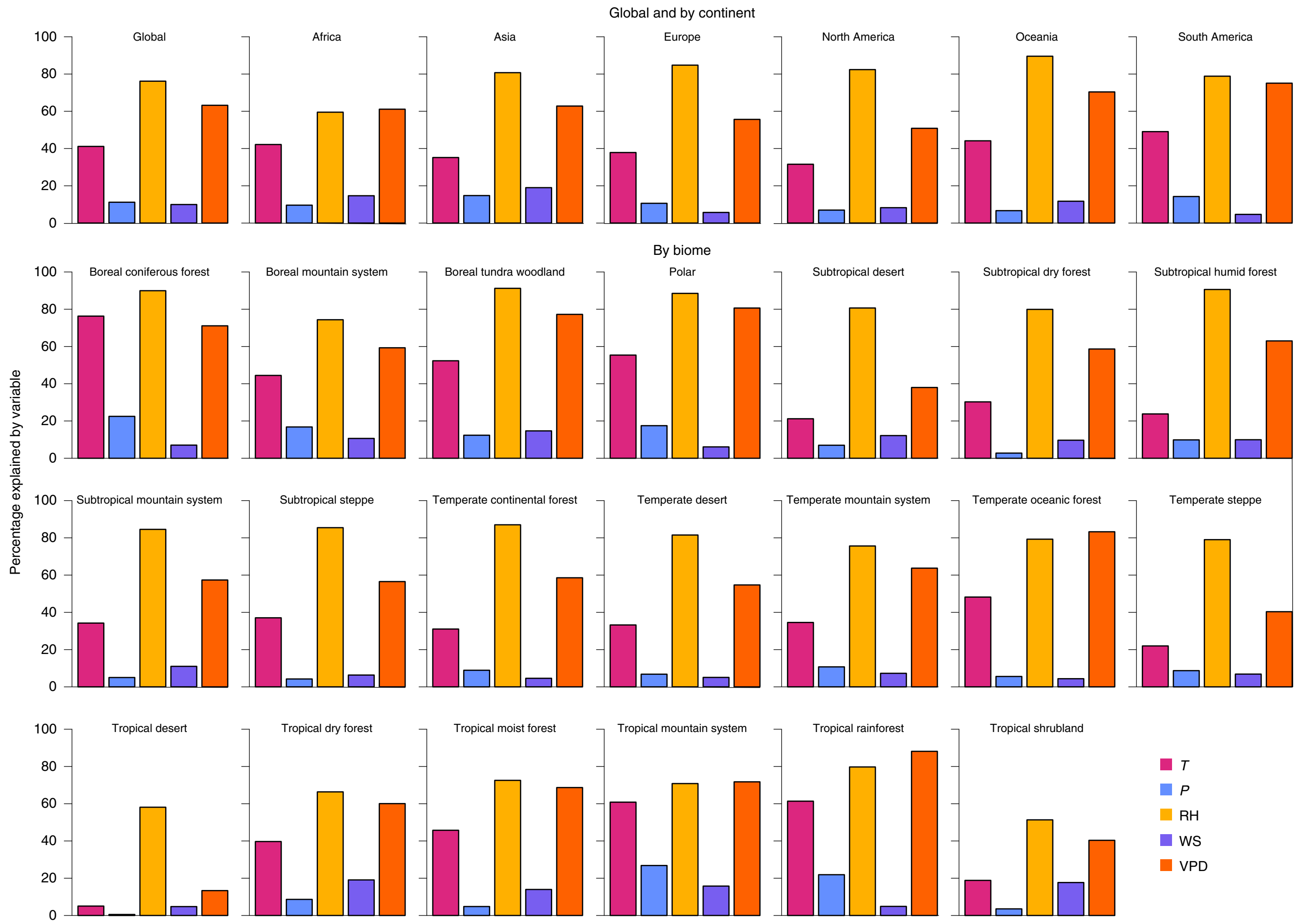

Fig. 4 | Attribution of FWI_{95} trends by region. Percentage of significant trends for FWI_{95} attributable to trends in FWI input variables T, precipitation (P), RH and WS, as well as VPD, summarized globally, by continent and by biome. Results were determined using the pMK test (Methods).

Because RH was the most frequent driver of significant trends in both FWI_{95} and ISI_{95}, we also examined the covariance of trends between these response variables and VPD (Fig. 4 and Supplementary Tables 3 and 6). Globally, VPD trends exhibited significant covariance with 61.6 and 59.1% of grid cells having significant trends in FWI_{95} and ISI_{95}, respectively We note that the direct usage of RH as an input variable in the CFWIS may explain its elevated importance as a driver of fire weather trends relative to VPD.

These findings are consistent with earlier global studies that documented the concurrence of observed fire weather trends with changes in weather variables[14]. Regional studies have also linked observed trends in fire weather to changes in meteorological variables[16–20]. However, only one study also employed a formal statistical test to attribute the drivers of observed regional fire weather trends[30]. Climate models have further illustrated the influence of changing meteorological variables on fire weather conditions at both the global[10,15] and regional scale[30,31]. These observation- and simulation-based studies predominantly found that T and RH were the main drivers of trends in fire weather and that changes in WS or precipitation played a minor role, which aligns well with our results. Our finding that decreasing RH is the most frequent driver of observed increases in extreme fire weather also aligns with projected decreases in RH over land with anthropogenic climate change[32]. The identification of location-specific drivers of extreme fire weather may inform the use of climate model output for projection of future fire weather indices.

Relationship between temperature, humidity and fire weather

The pMK trend attribution analysis presented here does not explicitly consider correlations between covariates. Notably, T is correlated with both RH and VPD, most directly through saturated vapour pressure (e_s), which represents the vapour pressure at which the air is in equilibrium with liquid water and the actual vapour pressure (e_a), which depends on the dew point temperature Td. The functional form of these quantities can be approximated by the Clausius–Clapeyron relation such that positive changes in temperature and negative changes in Td are always associated with increasing VPD (or decreasing RH). When changes in T and Td are in the same direction (for example, positive), the resulting changes in VPD (or RH) depend on the relative magnitudes of the underlying changes. To investigate these relationships, we further examined trends in the fire season 2 m noon T and Td, and their influence on trends in the extreme fire weather metrics considered here (Fig. 5a,b). Significant positive trends in T were found for 73.5% of global burnable land mass, with negative significant trends accounting for only 0.4%. In contrast, significant positive trends for Td were found for 44.3% of global burnable land mass, with negative significant trends found in 12.4% of burnable lands. Overall, locations with both positive T and Td trends occurred for 68.3% of all observed trends. Moreover, increasing T and decreasing Td accounted for 27.1% of all trends, decreasing T and increasing Td accounted for only 3.3% while both negative T and Td trends accounted for only

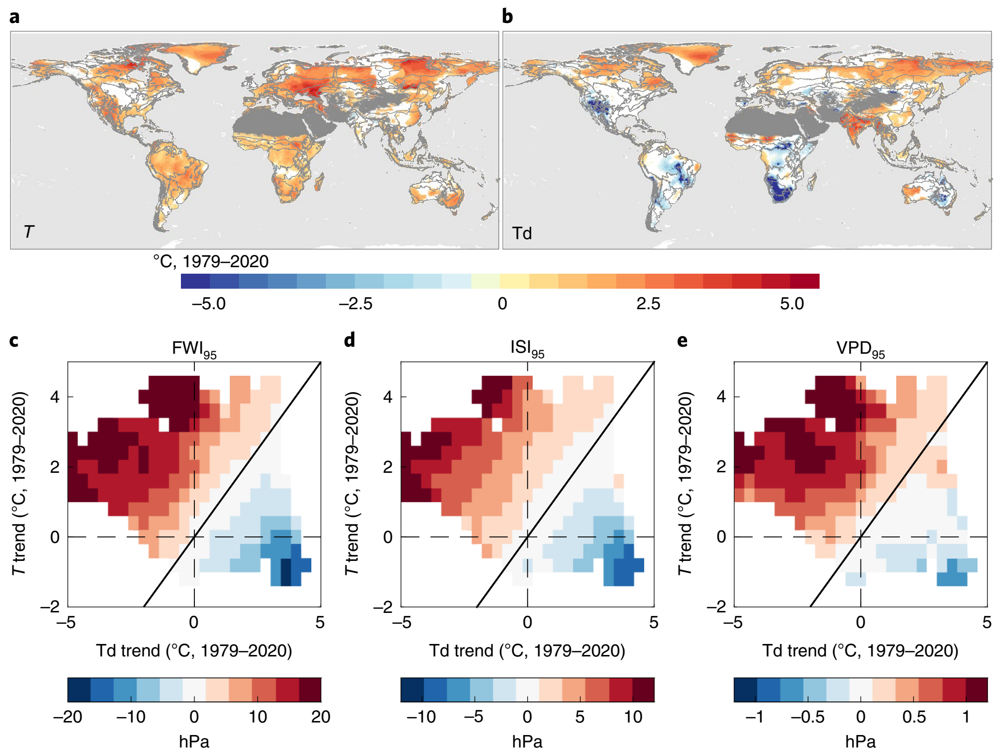

Fig. 5 | Trends in *T* and Td and relationship with extreme fire weather trends. a,b, Significant trends in mean 2-m *T* (**a**) and 2-m Td (**b**) over the fire season from 1979 to 2020. Light grey indicates the boundaries of biomes, modified from ref. [50] (Methods). **c–e**, Mean magnitude of significant trends in FWI_{95} (**c**), ISI_{95} (**d**) and VPD_{95} (**e**) are binned to show their dependence on trends in mean fire season *T* and Td. Diagonal black line indicates where trends in *T* equal those in Td.

1.3%. Interestingly, there were regional differences in directions of observed *T* and Td trends: some regions showed significant positive *T* trends and positive Td trends (for example, North America, Eurasian Boreal, India) whereas other regions recorded significant positive *T* trends and negative Td trends (for example, western USA, Amazon, southern Africa; Fig. 5a,b). These Td trends are consistent with observed atmospheric moisture trends found in other global studies[33,34] and in regional studies of the USA[35], Australia[36] and the Amazon[37].

In general, the moisture-holding capacity of the atmosphere increases by approximately 7% per 1°C of warming under climate change, assuming Clausius–Clapeyron scaling[33]. However, actual atmospheric moisture content is related to Td, which may not increase at the same rate. In fact, as we have observed here, Td trends are negative in many regions, which help further to drive increases in VPD (and decreases in RH) where temperatures are increasing. Regional differences in Td trends are strongly influenced by the terrestrial water cycle and can often be explained by vegetation–atmosphere dynamics or broad-scale land-use changes[38]. For example, in semi-arid regions such as in western North America, Australia and South Africa, evapotranspiration rates are strongly moisture limited[39] and land–atmosphere feedbacks can further enhance aridity under climate change[40]. Recent deforestation in the Amazon basin has also been linked to reduced evapotranspiration and increased VPD[37]; in contrast, increases in specific humidity in India have been driven by increased irrigation, particularly in the Indo-Gangetic Plain[41].

These regional differences for trends in *T* and Td underlie many of the observed variations in trends for extreme fire weather. To verify this, we also examined significant trends in FWI_{95}, ISI_{95} and VPD_{95} as a function of those in *T* and Td (Fig. 5c–e). For all three variables, positive trends co-occurred predominantly where *T* trends are greater in value than Td trends, a condition that occurred for 99.4, 99.3 and 90.9% of the identified positive significant trends in FWI_{95}, ISI_{95} and VPD_{95}, respectively, whereas this condition occurred for 73.5% of all global burnable lands; the strongest trends in these variables occurred where trends in *T* were positive and those in Td were negative.

Finally, we do not explicitly attribute observed changes in fire weather extremes to anthropogenic climate change in this study. While observed changes in meteorological variables and fire weather metrics largely reflect those in climate model simulations[10], observed regional differences in recent trends may also be tied to internal multi-decadal variability[42].

Discussion and conclusions

Our findings are important for several main reasons. First, our observational trend analysis extends the time period of earlier studies[14] and uses a modern global reanalysis dataset (ERA5)[21], which greatly improves both spatial resolution and accuracy compared with previous reanalyses. Second, in contrast to earlier studies, we have chosen to focus here on extreme fire weather, which is known to be responsible for the majority of large fire events[8]. Third, we statistically attributed the meteorological drivers of observed fire weather trends at the global scale. Better understanding of regional differences in fire weather trends and their drivers will help inform adaptation and mitigation strategies at scales appropriate for fire and land-use management. Our global study also provides insights into fire weather trends for lesser-studied fire-prone regions of the earth (for example, Asia, South America and Africa). Last, our findings that *T* and RH are driving observed global trends in fire weather are consistent with simulation-based studies[10,15]; in fact, these two variables generally have robust agreement among climate change projections in terms of thermodynamics[43]. This yields greater confidence in projections of future fire weather under global warming in spite of remaining uncertainties in projections of future precipitation and winds.

Wildfire management is challenging at the best of times, but the increasing demands on fire management agencies operating in complicated, multiple-use landscapes have made it even more difficult[44]. Many of the regions identified here as having positive trends in extreme fire weather have, in recent decades, experienced extreme wildfire events, some of which were disastrous[8]. We may see even more catastrophic fires in the future due to climate change, as we expect the increasing trend in extreme fire weather to cover more regions of the world and for fire weather to become even more extreme[7,45]. In addition to an increase in extreme fire weather, it is also likely that in the future there will be a greater number of wildland fire ignitions in some regions due to climate-driven increases in lightning activity, especially in the Arctic tundra and boreal forest ecosystem[46]. It is therefore distinctly possible that some of the regions displaying positive trends in extreme fire weather will face a future with more wildland fire. Without changes in fire management practices, climate change is therefore expected to increase the economic costs of fire suppression[47] and may lead to fire seasons that overwhelm fire suppression agencies[48,49]. Thus, although wildfire management is adaptive, substantive changes may be required in the future as the current status quo may no longer be a viable option in areas of the world facing increasing extreme fire weather.

In summary, our analysis based on three fire weather metrics (FWI, ISI and VPD) shows that extreme fire weather has significantly increased over a quarter to nearly half of the Earth's burnable surface over the past four decades (1979–2020), with important regional differences. Annual anomalies in the global means of extreme fire weather variables are highly correlated with global land-surface temperature anomalies, with the most recent decade containing the eight most extreme fire weather years on record. We have demonstrated that decreases in RH and increases in T were primarily responsible for increases in extreme fire weather globally; conversely, changes in WS and daily precipitation were contributing factors for relatively few trends. Furthermore, positive trends in fire weather extremes overwhelmingly occurred where trends in T outpace trends in Td. Our results are consistent with climate change studies, and extreme fire weather is likely to continue to increase, occur in more areas and become more severe in the future as the climate continues to warm.

Online content

Any methods, additional references, Nature Research reporting summaries, source data, extended data, supplementary information, acknowledgements, peer review information; details of author contributions and competing interests; and statements of data and code availability are available at https://doi.org/10.1038/s41558-021-01224-1.

Received: 5 June 2021; Accepted: 20 October 2021;
Published online: 25 November 2021

References

1. Abatzoglou, J. T., Williams, A. P., Boschetti, L., Zubkova, M. & Kolden, C. A. Global patterns of interannual climate-fire relationships (2018). *Glob. Change Biol.* **24**, 5164–5175 (2018).
2. Littell, J. S., McKenzie, D., Peterson, D. L. & Westerling, A. L. Climate and wildfire area burned in western US ecoprovinces, 1916-2003. *Ecol. Appl.* **19**, 1003–1021 (2009).
3. Abatzoglou, J. T. & Kolden, C. A. Relationships between climate and macroscale area burned in the western United States. *Int. J. Wildland Fire* **22**, 1003–1020 (2013).
4. Wang, X. et al. Projected changes in daily fire spread across Canada over the next century. *Environ. Res. Lett.* **12**, 025005 (2017).
5. Hanes, C. C. et al. Fire-regime changes in Canada over the last half century. *Can. J. Res.* **49**, 256–269 (2019).
6. Amiro, B. D. et al. Fire weather index system components of large fires in the Canadian boreal forest. *Int. J. Wildland Fire* **13**, 391–400 (2004).
7. Flannigan, M. D., Krawchuck, M. A., de Groot, W. J., Wotton, B. M. & Gowman, L. M. Implications of changing climate for global wildland fire. *Int. J. Wildland Fire* **18**, 483–507 (2009).
8. Bowman, D. M. J. S. et al. Human exposure and sensitivity to globally extreme wildfire events. *Nat. Ecol. Evol.* **1**, 0058 (2017).
9. Coogan, S. C. P., Robinne, F.-N., Jain, P. & Flannigan, M. D. Scientists' warning on wildfire—a Canadian perspective. *Can. J. Res.* **49**, 1015–1023 (2019).
10. Abatzoglou, J. T., Williams, A. P. & Barbero, R. Global emergence of anthropogenic climate change in fire weather indices. *Geophys. Res. Lett.* **46**, 326–336 (2019).
11. Van Wagner, C. E. et al. *Development and Structure of the Canadian Forest Fire Weather Index System* (Canadian Forestry Service Headquarters, 1987); https://www.eea.europa.eu/data-and-maps/indicators/forest-fire-danger-3/camia-et-al.-2008-past
12. Flannigan, M. D. & Harrington, J. B. A study of the relation of meteorological variables to monthly provincial area burned by wildfire in Canada (1953-80). *J. Appl. Meteorol.* **27**, 441–452 (1988).
13. Flannigan, M. D. et al. Fuel moisture sensitivity to temperature and precipitation: climate change implications. *Clim. Change* **134**, 59–71 (2016).
14. Jolly, W. M. et al. Climate-induced variations in global wildfire danger from 1979 to 2013. *Nat. Commun.* **6**, 7537 (2015).
15. Touma, D., Stevenson, S., Lehner, F. & Coats, S. Human-driven greenhouse gas and aerosol emissions cause distinct regional impacts on extreme fire weather. *Nat. Commun.* **12**, 212 (2021).
16. Clarke, H. G., Smith, P. L. & Pitman, A. J. Regional signatures of future fire weather over eastern Australia from global climate models. *Int. J. Wildland Fire* **20**, 550–562 (2011).
17. Bedia, J. et al. Sensitivity of fire weather index to different reanalysis products in the Iberian Peninsula. *Nat. Hazards Earth Syst. Sci.* **12**, 699–708 (2012).
18. Jain, P., Wang, X. & Flannigan, M. D. Trend analysis of fire season length and extreme fire weather in North America between 1979 and 2015. *Int. J. Wildland Fire* **26**, 1009–1020 (2017).
19. Dowdy, A. J. Climatological variability of fire weather in Australia. *J. Appl. Meteorol. Climatol.* **57**, 221–234 (2018).
20. Zhao, F., Liu, Y. & Shu, L. Change in the fire season pattern from bimodal to unimodal under climate change: the case of Daxing'anling in Northeast China. *Agric. Meteorol.* **291**, 108075 (2020).
21. Hersbach, H. et al. The ERA5 global reanalysis. *Q. J. R. Meteorol. Soc.* **146**, 1999–2049 (2020).
22. Abatzoglou, J. T. & Williams, A. P. Impact of anthropogenic climate change on wildfire across western US forests. *Proc. Natl Acad. Sci. USA* **113**, 11770–11775 (2016).
23. Kirchmeier-Young, M. C., Gillet, N. P., Zwiers, F. W., Cannon, A. J. & Anslow, F. S. Attribution of the influence of human-induced climate change on an extreme fire season. *Earths Future* **7**, 2–10 (2019).
24. Pausas, J. G. & Ribeiro, E. The global-fire productivity relationship. *Glob. Ecol. Biogeogr.* **22**, 728–736 (2013).
25. Cochrane, M. A. Fire science for rainforests. *Nature* **421**, 913–919 (2003).
26. Ziel, R. H. et al. A comparison of fire weather indices with MODIS fire days for the natural regions of Alaska. *Forests* **11**, 516 (2020).
27. Giannaros, T. M., Kotroni, V. & Lagouvardos, K. Climatology and trend analysis (1987–2016) of fire weather in the Euro-Mediterranean. *Int. J. Climatol.* **41**, E491–E508 (2021).
28. Harris, S. & Lucas, C. Understanding the variability of Australian fire weather between 1973 and 2017. *PLoS ONE* **14**, e0222328 (2019).
29. *Climate at a Glance* (NOAA, 2021); https://www.ncdc.noaa.gov/cag/
30. van Oldenborgh, G. J. et al. Attribution of the Australian bushfire risk to anthropogenic climate change. *Nat. Hazards Earth Syst. Sci.* **21**, 941–960 (2021).
31. Barbero, R., Abatzoglou, J. T., Pimont, F., Ruffault, J. & Curt, T. Attributing increases in fire weather to anthropogenic climate change over France. *Front. Earth Sci.* https://doi.org/10.3389/feart.2020.00104 (2020).
32. Byrne, M. P. & O'Gorman, P. A. Understanding decreases in land relative humidity with global warming: conceptual model and GCM simulations. *J. Clim.* **29**, 9045–9061 (2016).
33. Willett, K. M., Jones, P. D., Gillett, N. P. & Thorne, P. W. Recent changes in surface humidity: development of the HadCRUH dataset. *J. Clim.* **21**, 5364–5383 (2008).
34. Matsoukas, C. et al. Potential evaporation trends over land between 1983-2008: driven by radiative fluxes or vapour-pressure deficit? *Atmos. Chem. Phys.* **11**, 7601–7616 (2011).
35. Grotjahn, R. & Huynh, J. Contiguous US summer maximum temperature and heat stress trends in CRU and NOAA climate division data plus comparisons to reanalyses. *Sci. Rep.* **8**, 11146 (2018).
36. Denson, E., Wasko, C. & Peel, M. C. Decreases in relative humidity across Australia. *Environ. Res. Lett.* https://doi.org/10.1088/1748-9326/ac0aca (2021).

37. Barkhordarian, A., Saatchi, S. S., Behrangi, A., Loikith, P. C. & Mechoso, C. R. A recent systematic increase in vapor pressure deficit over tropical South America. *Sci. Rep.* **9**, 15331 (2019).
38. Findell, K. L. et al. The impact of anthropogenic land use and land cover change on regional climate extremes. *Nat. Commun*. **8**, 989 (2017).
39. McKinnon, K. A., Poppick, A. & Simpson, I. R. Hot extremes have become drier in the United States Southwest. *Nat. Clim. Change* https://doi.org/10.1038/s41558-021-01076-9 (2021).
40. Berg, A. et al. Land–atmosphere feedbacks amplify aridity increase over land under global warming. *Nat. Clim. Change* **6**, 869–874 (2016).
41. Mishra, V. et al. Moist heat stress extremes in India enhanced by irrigation. *Nat. Geosci.* **13**, 722–728 (2020).
42. Dong, B. & Dai, A. The influence of the interdecadal Pacific oscillation on temperature and precipitation over the globe. *Clim. Dyn.* **45**, 2667–2681 (2015).
43. Fischer, E. M. & Knutti, R. Robust projections of combined humidity and temperature extremes. *Nat. Clim. Change* **3**, 126–130 (2013).
44. Tymstra C., Flannigan M. D., Stocks B. J., Cai X. & Morrison K. Wildfire management in Canada: review, challenges and opportunities. *Prog. Disaster Sci*. https://doi.org/10.1016/j.pdisas.2019.100045 (2020).
45. Flannigan, M. D., Stocks, B., Turetsky, M. & Wotton, M. Impacts of climate change on fire activity and fire management in the circumboreal forest. *Glob. Change Biol.* **15**, 549–560 (2009).
46. Chen, Y. et al. Future increases in Arctic lightning and fire risk for permafrost carbon. *Nat. Clim. Change* https://doi.org/10.1038/s41558-021-01011-y (2021).
47. Hope, E. S., McKenney, D. W., Pedlar, J. H., Stocks, B. J. & Gauthier, S. Wildfire suppression costs for Canada under a changing climate. *PLoS ONE* **11**, e0157425 (2016).
48. Podur, J. & Wotton, B. M. Will climate change overwhelm fire management capacity? *Ecol. Modell.* **221**, 1301–1309 (2010).
49. Abatzoglou, J. T., Juang, C. S., Williams, A. P., Kolden, C. A. & Westerling, A. L. Increasing synchronous fire danger in forests of the western United States. *Geophys. Res. Lett.* **48**, e2020GL091377 (2021).
50. Olson, D. M. et al. Terrestrial ecoregions of the world: a new map of life on Earth. *Bioscience* **51**, 933–938 (2001).

Publisher's note Springer Nature remains neutral with regard to jurisdictional claims in published maps and institutional affiliations.

Methods

Data. We used the recently released ERA5 reanalysis data[21] to provide the meteorological variables required for input into the calculation of the CFWIS variables, including FWI and ISI. The ERA5 global reanalysis is a fifth-generation product, produced by the European Centre for Medium-range Weather Forecasts, that replaced ERA-Interim. The large spatial coverage of reanalysis data typically offers a better alternative to weather station data for larger-scale analyses such as this, while the ERA5 reanalysis offers several improvements over earlier reanalysis products and its predecessor, ERA-Interim[21,51]. One key improvement is that ERA5 offers much higher spatial and temporal resolution by providing hourly analysis fields for 137 levels (from the surface up to a height of 80 km) on a 31-km horizontal grid. Various studies have shown that ERA5 improves on other surface weather reanalyses with respect to WS[52], precipitation[53] and hydrological modelling[54], for example. It should be noted, however, that there are uncertainties in regard to WS values and their trends between various reanalyses that may bias fire weather calculations[55]. We downloaded ERA5 hourly single-pressure-level (surface) data for the period 1979–2020 (available from https://cds.climate.copernicus.eu/cdsapp#!/dataset/reanalysis-era5-single-levels?tab=overview).

We defined global regions based on the biome categorization from ref. [50], which captures homogeneous climate and vegetation characteristics at a broad scale and is therefore appropriate for determination of fire regimes and fire seasons for global-scale studies. Biomes of >1,000,000 ha were split into smaller ecoregions based on the latest classification from the World Wildlife Fund[56]. In total we partitioned the globe into 20 biomes (Fig. 1a), with further stratification by continent resulting in 105 distinct regions (biomes × continents).

We downloaded global fire data from the Global Fire Atlas (GFA), which is based on the MODIS satellite record[57], for estimation of fire season length for each biome (below). The GFA provided day of burn at 500-m resolution for each year for the period 2003–2016. Many regions of the globe were affected by wildfires each year, as indicated by the mean annual percentage of area burned by biome (Fig. 1b).

FWI calculation. We used the ERA5 reanalysis to estimate the CFWIS variables ISI and FWI for our global trend analysis. Both ISI and FWI provide numeric ratings of relative wildland fire potential using surface weather variables as inputs, and are based on tracking moisture in three fuel layers of varying depth with corresponding moisture codes: fine fuel moisture code (FFMC, litter and fine fuels), Duff moisture code (organic fuels at moderate depth) and drought code (deep and compact organic fuels). The calculation of these CFWIS components is based on daily observations of T, RH, WS and 24-h accumulated precipitation[11]. The ISI combines WS and FFMC to give an index of a fire's rate of spread and is a useful indicator across a range of forest types[58]. The FWI index combines ISI and the build-up index (a measure of cumulative fuel dryness) and represents potential fire intensity[6,12]. Although the CFWIS was originally developed for use in the Canadian boreal forest, it has been calibrated for use in many regions and has also found global application in several research studies[1,14,59,60]. The FWI has strong positive correlations with area burned across the majority of global burnable land mass, but the relationship is weaker in arid ecosystems[1,60]. However, it should be noted that both ISI and FWI, like all CFWIS variables, are qualitative—fuel type needs to be accounted for to generate quantitative values of fire behaviour, and they do not incorporate changes in other elements of fire potential.

The ERA5 meteorological data required preprocessing before calculation of FWI and ISI. For T, we used 2-m T, where units were converted from K to °C. We calculated 2-m RH from 2-m T and 2m Td based on equations 1 and 2 in ref. [61]. We calculated 10-m WS in km h^{-1} from the 10-m U (zonal velocity) and V (meridional velocity) wind components, as required by the FWI system. Finally, we used hourly total precipitation to calculate 24-h accumulated precipitation, which was converted to units of millimetres. All variables were obtained for noon local time to provide daily inputs as required for the FWI system calculations.

Using these inputs, we calculated ISI and FWI according to the procedure outlined in ref. [61]. In particular, an overwintering procedure was applied to adjust the spring start-up value of the drought code based on the amount of overwinter precipitation for regions with seasonal snow cover. A meteorological proxy for continuous snow cover at each grid cell was used to determine when to start and stop the calculation. Specifically, maximum daily T (T_{max}) was used to determine when the FWI calculation was to be deactivated (after 3 consecutive days with T_{max} <5 °C) or reactivated (after 3 consecutive days with T_{max} >12 °C), as per ref. [62].

Fire season estimation. Because we were interested in fire weather trends during the fire season, we estimated the observed fire season for each biome using data from the Global Fire Atlas[57]. We aggregated the day of burn fire data (2003–2016) over each biome and then defined the biome-level fire season as the minimum number of months accounting for at least 90% of the area burned for each biome (Supplementary Table 1). Although we used fixed fire seasons for our analysis, it should be noted that these may change over time because there have been observed increases in fire season length in several regions as well as globally[14,18].

VPD. We also examined trends in VPD, a metric that provides a measure of the atmosphere's capacity to extract moisture from surface vegetation. Several studies have found linkages between VPD and fire ignitions, growth and burned area[63–66]. VPD was calculated using hourly ERA5 2-m T and 2-m Td using the conversion equation from ref. [67] and implemented in the R package bigleaf[68].

Trend analysis. We examined trends in the time series of ISI_{95}, FWI_{95} and VPD_{95} values at each grid cell, globally. Annual values were calculated at each grid cell and for each biome from 1979 to 2020 (42 years in total). In each case, the annual percentile values included only data contained in the observed fire season months. We further masked out barren areas using land-cover MODIS satellite data[69] and defined according to the International Geosphere-Biosphere Program land-cover classification system[70], because these areas did not contain significant burnable biomass and many would otherwise skew the results due to their highly arid climate (for example, North Africa). Trend analysis was performed on the time series using the Mann–Kendall (MK) test, a robust non-parametric test for trend detection[71,72]. Linear trends were determined using the Theil–Sen estimator[73,74]. We tested for both temporal and spatial autocorrelation and found the data to be spatially autocorrelated, as expected with climate data. It is well known that the presence of autocorrelation can lead to the detection of spurious trends[75]. Here multiple testing and spatial autocorrelation were respectively accounted for by controlling the false discovery rate (FDR)[76] and by setting the global significance level (α_{global}) equal to 0.5 α_{FDR} (ref. [77]); here we set α_{global} to 0.05. We display the results of our significant trends in Figs. 2, 3 and 4 at this significance level. The 95th percentiles we examined represent extreme values in fire weather metrics, however, and we also examined trends in the 50th and 75th percentiles and found similar results (Supplementary Figs. 3 and 4), indicating that our results are not overly sensitive to the choice of percentile.

Drivers of trends in FWI_{95} and ISI_{95}. We used the pMK test to assess the influence of covariates on the trend of our response variables[78]. The pMK test modifies the MK test by removing the contribution of a covariate of interest that correlates with the response variable. If any trend in the response variable that was originally determined to be statistically significant is no longer significant (here, tested at the $\alpha = 0.05$ level) after accounting for the covariate and repeating the test, then the covariate has a significant influence on the detected trend; in this case, we refer to the corresponding covariate as a driver of a significant trend in the response variable. For example, ref. [79] used this method to link trends in flood metrics to increases in evapotranspiration. Here, because the four FWI inputs (T, RH, WS and precipitation) can combine nonlinearly to generate FWI outputs, the association between FWI_{95} or ISI_{95} and the upper (or lower) annual quantiles of the inputs may not necessarily be strong. To determine the influence of each of the inputs, we extracted input values that corresponded to the response variable (for example, FWI_{95} or ISI_{95}) of interest; this was achieved by binning all input values corresponding to values of the response variable in a range centred on the 95th percentile (92.5–97.5%) and taking the median value of each of the binned inputs. Note that the pMK test we used to determine drivers of FWI_{95} and ISI_{95} is a test that determines whether trends in covariates display significant covariance with observed trends, but is not equivalent to a sensitivity analysis[13,80]. It should further be noted that because multiple covariates can be drivers of observed trends, the attribution percentages summed over all variables considered can be >100%.

The MK and pMK tests were performed using the R packages EnvStats[81] and trend[82]. FDR correction was applied using the p.adjust function in the R base stats package. All analyses were performed using R v.4.0.1.

Data availability

The hourly ERA5 data used for this study are available at https://doi.org/10.24381/cds.adbb2d47. The fire weather metrics derived for the period 1979–2020 that support the findings of this study are available from https://doi.org/10.5281/zenodo.5567021 (daily ISI and FWI) and https://doi.org/10.5281/zenodo.5567062 (daily maximum VPD). Global mean land-surface temperatures are available from the NOAA National Centers for Environmental information, Climate at a Glance: Global Time Series (published July 2021), at https://www.ncdc.noaa.gov/cag/. The global biomes used in this study are available at https://www.worldwildlife.org/publications/terrestrial-ecoregions-of-the-world and land-cover data are available at https://doi.org/10.5067/MODIS/MCD12Q1.006.

References

51. *Copernicus Climate Change Service Data Store* (Copernicus Climate Change Service, accessed 4 March 2020); https://confluence.ecmwf.int/display/CKB/ERA5%3A+data+documentation
52. Ramon, J., Lledo, L., Torralba, V., Soret, A. & Doblas-Reyes, F. J. What global reanalysis best represents near-surface winds? *Q. J. R. Meteorol. Soc.* **145**, 3236–3251 (2019).
53. Beck, H. E. et al. Daily evaluation of 26 precipitation datasets using stage-IV gauge-radar data for the CONUS. *Hydrol. Earth Syst. Sci.* **23**, 207–224 (2019).
54. Tarek, M., Brissette, F. P. & Arsenault, R. Evaluation of the ERA5 reanalysis as a potential reference dataset for hydrological modelling over North America. *Hydrol. Earth Syst. Sci.* **24**, 2527–2544 (2020).
55. Torralba, V., Doblas-Reyes, F. J. & Gonzalez-Reviriego, N. Uncertainty in recent near-surface wind speed trends: a global reanalysis intercomparison. *Environ. Res. Lett.* **12**, 114019 (2017).

56. Dinerstein, E. et al. An ecoregion-based approach to protecting half the terrestrial realm. *BioScience* **67**, 534–545 (2017).
57. Andela, N. et al. The global fire atlas of individual fire size, duration, speed and direction. *Earth Syst. Sci. Data* **11**, 529–552 (2019).
58. Wotton, B. M. Interpreting and using outputs from the Canadian Forest Fire Danger Rating System in research applications. *Environ. Ecol. Stat.* **16**, 107–131 (2009).
59. Field, R. D. et al. Development of a global fire weather database. *Nat. Hazards Earth Syst. Sci.* **15**, 1407–1423 (2015).
60. Bedia, J. et al. Global patterns in the sensitivity of burned area to fire weather: implications for climate change. *Agric. Meteorol.* **214–215**, 369–379 (2015).
61. McElhinny, M., Beckers, J. F., Hanes, C., Flannigan, M. & Jain, P. A high-resolution reanalysis of global fire weather from 1979 to 2018 – overwintering the Drought Code. *Earth Syst. Sci. Data* **12**, 1823–1833 (2020).
62. Wotton, B. M. & Flannigan, M. D. Length of the fire season in a changing climate. *Forestry Chron.* **69**, 187–192 (1993).
63. Sedano, F. & Randerson, J. T. Vapor pressure deficit controls on fire ignition and fire spread in boreal forest ecosystems. *Biogeosciences* **11**, 1309–1353 (2014).
64. Williams, P. A. et al. Correlations between components of the water balance and burned area reveal new insights for predicting forest fire area in the southwest United States. *Int. J. Wildland Fire* **24**, 14–26 (2014).
65. Williams, A. P. et al. Observed impacts of anthropogenic climate change on wildfire in California. *Earths Future* **7**, 892–910 (2019).
66. Mueller, S. E. et al. Climate relationships with increasing wildfire in the southwestern US from 1984 to 2015. *For. Ecol. Manage.* **460**, 117861 (2020).
67. Alduchov, O. A. & Eskridge, R. E. Improved Magnus form approximation of saturation vapor pressure. *J. Appl. Meteorol.* **35**, 601–609 (1996).
68. Knauer, J., El-Madany, T. S., Zaehle, S. & Migliavacca, M. Bigleaf—an R package for the calculation of physical and physiological ecosystem properties from eddy covariance data. *PLoS ONE* **13**, e0201114 (2018).
69. Friedl, M. A. et al. MODIS Collection 5 global land cover: algorithm refinements and characterization of new datasets. *Remote Sens. Environ.* **114**, 168–182 (2010).
70. Loveland, T. R. & Belward, A. S. The IGBP-DIS global 1 km land cover data set, DISCover: first results. *Int. J. Remote Sens.* **18**, 3291–3295 (1997).
71. Mann, H. B. Nonparametric tests against trend. *Econometrica* **13**, 245–259 (1945).
72. Kendall, M. G. *Rank Correlation Methods* (Griffin, 1975).
73. Theil, H. A rank-invariant method of linear and polynomial regression analysis. I, II, III. *Nederl. Akad. Wetensch. Proc.* **53**, part I: 386–392; part II: 521–525; part III: 1397–1412 (1950).
74. Sen, P. K. Estimates of the regression coefficient based on Kendall's tau. *J. Am. Stat. Assoc.* **63**, 1379–1389 (1968).
75. Yue, S., Pilon, P. & Phinney, B. Canadian streamflow trend detection: impacts of serial and cross-correlation. *Hydrol. Sci. J.* **48**, 51–63 (2003).
76. Wilks, D. S. On 'field significance' and the false discovery rate. *J. Appl. Meteorol. Climatol.* **45**, 1181–1189 (2006).
77. Wilks, D. 'The stippling shows statistically significant grid points': how research results are routinely overstated and overinterpreted, and what to do about it. *Bull. Am. Meteorol. Soc.* **97**, 2263–2273 (2016).
78. Libiseller, C. & Grimvall, A. Performance of partial Mann–Kendall tests for trend detection in the presence of covariates. *Environmetrics* **13**, 71–84 (2002).
79. Mediero, L., Santillán, D., Garrote, L. & Granados, A. Detection and attribution of trends in magnitude, frequency and timing of floods in Spain. *J. Hydrol.* **517**, 1072–1088 (2014).
80. Dowdy, A. J., Mills, G. A., Finkele, K. & de Groot, W. Index sensitivity analysis applied to the Canadian Forest Fire Weather Index and the McArthur Forest Fire Danger Index. *Meteorol. Appl.* **17**, 298–312 (2010).
81. Millard, S. P. *EnvStats: An R Package for Environmental Statistics* (Springer, 2013).
82. Pohlert, T. *trend: Non-Parametric Trend Tests and Change-Point Detection*. R package v.1.1.4. https://CRAN.R-project.org/package=trend (2020).

Acknowledgements
We thank the Canadian Partnership for Wildland Fire Science for their support. P.J. thanks M. McElhinny and J. Beckers for their help in developing code for FWI calculation. J.T.A. was partially supported by NSF award no. OAI-2019762.

Author contributions
P.J. and M.D.F. designed the initial study. All authors contributed to discussions regarding further development of the study design and analysis. D.C-A., P.J. and J.T.A. performed the analysis. S.C.P.C. and P.J. wrote the manuscript. All authors contributed to review and revision of the manuscript.

Competing interests
The authors declare no competing interests.

Additional information
Supplementary information The online version contains supplementary material available at https://doi.org/10.1038/s41558-021-01224-1.

Correspondence and requests for materials should be addressed to Piyush Jain.

Peer review information *Nature Climate Change* thanks Ubirajara Oliveira and the other, anonymous, reviewer(s) for their contribution to the peer review of this work.

Reprints and permissions information is available at www.nature.com/reprints.